

This discussion paper is/has been under review for the journal Atmospheric Measurement Techniques (AMT). Please refer to the corresponding final paper in AMT if available.

Volcanic ash infrared signature: realistic ash particle shapes compared to spherical ash particles

A. Kylling¹, M. Kahnert^{2,3}, H. Lindqvist⁴, and T. Nousiainen^{4,5}

¹NILU – Norwegian Institute for Air Research, P.O. Box 100, 2027 Kjeller, Norway

²Research Department, Swedish Meteorological and Hydrological Institute, Folkborgsvägen 17, 60176 Norrköping, Sweden

³Department of Earth and Space Science, Chalmers University of Technology, 41296 Gothenburg, Sweden

⁴Department of Physics, P.O. Box 48, 00014 University of Helsinki, Finland

⁵Finnish Meteorological Institute, P.O. Box 503, 00101 Finland

Received: 19 August 2013 – Accepted: 27 September 2013 – Published: 16 October 2013

Correspondence to: A. Kylling (arve.kylling@nilu.no)

Published by Copernicus Publications on behalf of the European Geosciences Union.

Title Page

Abstract

Introduction

Conclusions

References

Tables

Figures

◀

▶

◀

▶

Back

Close

Full Screen / Esc

Printer-friendly Version

Interactive Discussion



Abstract

The reverse absorption technique is often used to detect volcanic clouds from thermal infrared satellite measurements. From these measurements particle size and mass loading may also be estimated using radiative transfer modelling. The radiative transfer 5 modelling usually assumes that the ash particles are spherical. We calculate thermal infrared optical properties of highly irregular and porous ash particles and compare these with mass- and volume-equivalent spherical models. Furthermore, brightness temperatures pertinent to satellite observing geometry are calculated for the different ash particle shapes. Non-spherical shapes and volume-equivalent spheres are found to 10 produce a detectable ash signal for larger particle sizes than mass-equivalent spheres. The assumption of mass-equivalent spheres for ash mass loading estimates will underestimate the mass loading by several tens of percent compared to morphologically complex inhomogeneous ash particles.

1 Introduction

15 The difference between brightness temperatures (dBT) at 11 (BT11) and 12 μm (BT12) is often used to detect volcanic ash from space (Prata, 1989). For volcanic ash clouds dBT (= BT11 – BT12) is negative in contrast to liquid water and ice clouds which give positive dBT. For spherical ash particles the radii have to be below 5 μm to give a negative brightness temperature difference (Wen and Rose, 1994, using monodispersed 20 particle distributions). For retrieval of ash mass loading and effective radius, it is common to assume that the ash particles are spherical and thus use Mie theory to calculate the optical properties (extinction cross section, single scattering albedo and asymmetry factor) (e.g. Prata, 1989; Prata and Prata, 2012; Wen and Rose, 1994; Clarisse et al., 2010; Pavolonis et al., 2013). The optical properties of non-spherical particles can be 25 significantly different from spherical particles (see for example Mishchenko, 2009, and references therein). The non-sphericity of particles residing in the Earth's atmosphere

Infrared signature of realistic volcanic ash particles

A. Kylling et al.

[Title Page](#)

[Abstract](#)

[Introduction](#)

[Conclusions](#)

[References](#)

[Tables](#)

[Figures](#)

[◀](#)

[▶](#)

[Back](#)

[Close](#)

[Full Screen / Esc](#)

[Printer-friendly Version](#)

[Interactive Discussion](#)



may affect the signal measured by satellites and as such have an impact on the quantity which is being remotely sensed, e.g. the mass of a volcanic ash cloud.

Krotkov et al. (1999) used randomly oriented spheroids to test the sensitivity of Total Ozone Mapping Spectrometer (TOMS) retrieval of ash cloud optical depth and effective radius. The TOMS observes backscattered solar radiation in the 0.34–0.38 μm spectral interval. The assumption of spherical particles underestimates the effective radius by up to 30 % and overestimates the optical depth by up to 25 %. The total mass of the ash cloud is underestimated by 5–20 %. The UV volcanic ash refractive index used in that study, $m = 1.5 - 0.005i$, is different from that found in the thermal infrared where both the real and imaginary parts of the refractive index are higher (e.g. $m = 2.16 - 0.42i$ at 11 μm and $m = 1.83 - 0.13i$ at 12 μm for andesite according to Pollack et al., 1973). For a refractive index with a larger imaginary part (larger absorption), the electromagnetic field will not penetrate that far into the particle. Also, the roughness of the particle, not considered by Krotkov et al. (1999), may play an important role if the material is optically hard (large real part) and strongly absorbing (e.g. Kahnert et al., 2011, 2012). Finally, TOMS measures solar radiation backscattered by the atmosphere and its constituents, while infrared (IR) detectors, such as the Spinning Enhanced Visible and Infrared Imager (SEVIRI), measure the radiation emitted by the Earth's surface and atmosphere. Thus, the results in the UV may not be directly transferable to the thermal infrared.

To our knowledge only Newman et al. (2012) have investigated the effects of non-sphericity of ash particles in the infrared. They compared optical properties of equal volume spheres with those of randomly oriented hexagonal columns of unity aspect ratio as calculated by the T-matrix method. Differences between optical properties of the spheres and the hexagonal columns were reported to be less than 10 % which was considered not significant for their purposes (lidar-derived aerosol extinction and ash mass concentration to be used in a radiative closure study). It is noted that Yang et al. (2007) have compared radiative properties of dust-like spheroids and spheres at thermal infrared wavelengths and concluded that the effect of nonsphericity was not

Infrared signature of realistic volcanic ash particles

A. Kylling et al.

Title Page

Abstract

Introduction

Conclusions

References

Tables

Figures

|◀

▶|

◀

▶|

Back

Close

Full Screen / Esc

Printer-friendly Version

Interactive Discussion



significant. They based their conclusion on comparisons of brightness temperatures from simulations with spheres and spheroids and did not estimate the error on retrieved quantities.

The aim of the present study is to investigate how highly irregular and porous ash particles affect the thermal radiation measured by satellites and the possible impact on derived quantities such as ash mass loading. This is achieved by performing thermal infrared radiative transfer calculations with ash particles and comparing with calculations using spherical particles. The calculation of the optical properties of the ash particles, including description of their shapes, is outlined in Sect. 2. The radiative transfer calculations are described in Sect. 3 and the results are presented in Sect. 4. A discussion follows in Sect. 5 before conclusions are drawn.

2 Calculation of ash particle optical properties

To calculate the ash particle optical properties, model geometries for the ash particles are first generated. These geometries are then used in the single-scattering computations.

2.1 Particle shapes

Two distinct ash particle geometries are considered: vesicular ash particle shapes from Lindqvist et al. (2011) and porous spheroids from Nousiainen et al. (2011). The former model results in irregularly shaped particles, while in the latter the overall shape of the particles is spheroidal. Both types of particles are porous, that is, the generated model particles have hollow internal cavities.

In case of vesicular ash particles, we consider particles with both small and large vesicles (porous cavities). The generation of these shapes begins with a ballistic cluster of 40 (for large vesicles) or 500 (for small vesicles) spheres. The sizes of the spheres

[Title Page](#)

[Abstract](#)

[Introduction](#)

[Conclusions](#)

[References](#)

[Tables](#)

[Figures](#)

[◀](#)

[▶](#)

[◀](#)

[▶](#)

[Back](#)

[Close](#)

[Full Screen / Esc](#)

[Printer-friendly Version](#)

[Interactive Discussion](#)



follow a power-law size distribution

$$n(r) = \frac{2r_{\max}r_{\min}}{r_{\max}^2 - r_{\min}^2} r^{-3}, \quad (1)$$

where the maximum radius $r_{\max} = 4.0 r_{\min}$ for large vesicles and $r_{\max} = 2.0 r_{\min}$ for small vesicles. In the case of the large-vesicle particles, the ballistic clustering algorithm is modified to produce denser clusters such that for every ten spheres, only the sphere closest to the origin is chosen. Once the cluster has been formed, it is enveloped in a concave surface by the concave-hull transformation (Lindqvist et al., 2009), where a generating sphere of radius r_g (for large vesicles $r_g = 0.5 r_{\max}$, and for small $r_g = r_{\max}$) is rolled around the cluster and the inner surface shaped by this sphere defines the enveloping concave hull. Then, each sphere in the cluster is replaced by a co-centered Gaussian random sphere. These are stochastic, statistically deformed spheres which can be defined using, e.g., a power-law index v and a standard deviation of radial distance σ (Muinonen et al., 2007). The values chosen for the ash particles are $\sigma = 0.2$ and $v = 4.0$. The space outside the Gaussian random spheres and inside the concave hull form the ash particle, the Gaussian spheres defining the porous cavities. Since the Gaussian spheres are non-spherical, neighbouring Gaussian spheres may overlap, resulting in connected vesicles. To complete the ash particles, a shallow surface layer is removed from the particle, so that some vesicles are exposed. The parameter values for these phenomenological model particles have been selected based on visually inspecting scanning-electron microscope images of real volcanic ash particles.

Porous spheroids have the shape of normal spheroids, but they are filled with spherical vesicles. Again, we consider model shapes with both large and small vesicles. The porous spheroids are generated as follows. First, a ballistic cluster of 150 spheres (large vesicles) or 500 spheres (small vesicles) is built. Again, the modified version of the ballistic cluster algorithm from (Lindqvist et al., 2009) is used for a denser cluster. The sizes of the spheres vary according to the power-law size distribution in Eq. (1)

[Title Page](#)[Abstract](#)[Introduction](#)[Conclusions](#)[References](#)[Tables](#)[Figures](#)[|◀](#)[▶|](#)[◀](#)[▶|](#)[Back](#)[Close](#)[Full Screen / Esc](#)[Printer-friendly Version](#)[Interactive Discussion](#)

with a maximum radius $r_{\max} = 1.5 r_{\min}$. In case of large vesicles, both r_{\max} and r_{\min} are twice as large than in the case of small vesicles. Then, a spheroidal volume is overlaid, co-centered with the origin of the spherical cluster, and the interior of the spheroid is filled with material, save for the spheres. Everything outside the spheroidal volume is deleted. Four spheroids have been generated for the simulations: aspect ratio 1.5 prolate spheroid and aspect ratio 2.0 oblate spheroid, both with either small or large vesicles.

The porosity p of a particle describes the fractional volume of the cavities within the particle. For the large-vesicle ash shapes, porosity varies between $p = 0.41\text{--}0.60$ and, for small-vesicle ash, $p = 0.29\text{--}0.31$. Both spheroids with small cavities have porosity $p = 0.44$ while the porosity of large-cavity spheroids is $p = 0.48\text{--}0.50$.

In Fig. 1 the various ash particle shapes are presented: ash particles with large vesicles (left column), small vesicles (middle column) and prolate and oblate spheroids with large and small vesicles (right column). For details of the model particle generation, we refer to the original publications by Lindqvist et al. (2011) and Nousiainen et al. (2011).

2.2 Single scattering optical properties

The optical properties of the non-spherical ash particles were calculated by the discrete dipole approximation (DDA), using the DDSCAT program (Draine and Flatau, 1994, 2012). Calculations of the optical properties for the 14 geometries in Fig. 1 were made for 10 sizes of $1, 2, \dots, 10 \mu\text{m}$, and for 2 IR wavelengths, 11 and $12 \mu\text{m}$.

For comparison, computations for size-equivalent spheres were performed with a standard Mie program (Mishchenko et al., 2002). We considered different measures of size-equivalence:

1. Mass-equivalent spheres with the same refractive index as andesite. In this case, the radius of the spheres is calculated from the andesite volume V in the ash particles given by $V = Nd^3$, where N is the number of dipoles used to represent the target, and d^3 is the volume of each dipole cell. The vesicles are vacuum,

[Title Page](#)[Abstract](#)[Introduction](#)[Conclusions](#)[References](#)[Tables](#)[Figures](#)[|◀](#)[▶|](#)[◀](#)[▶|](#)[Back](#)[Close](#)[Full Screen / Esc](#)[Printer-friendly Version](#)[Interactive Discussion](#)

so only the dipoles of the mineral material contribute to N . The mass-equivalent radius R_m is then obtained from $(4/3)\pi R_m^3 = Nd^3$. It is noted that DDSCAT defines the extinction efficiency Q_{ext} in terms of the extinction cross section C_{ext} according to $Q_{\text{ext}} = C_{\text{ext}}/(\pi \cdot R_m^2)$, and similarly for the scattering efficiency Q_{sca} .

5 2. Volume-equivalent spheres. Here, we estimate the total volume V_{tot} of the particle (andesite and vesicles), and define the volume-equivalent radius R_v of the sphere by $(4/3)\pi R_v^3 = V_{\text{tot}}$. The spheres are treated as a homogeneous mixture of andesite and vacuum. We therefore need to compute an effective refractive index of this mixture based on the andesite volume fraction. By considering all five stochastic realisations of each class of particles (small and large vesicles), we obtain average andesite volume fractions of

- 10 50 % for particles with large vesicles
- 15 70 % for particles with small vesicles.

15 The vesicles were assumed to be “vacuum”, i.e. they have a refractive index of $m = 1$. In each case an effective refractive index was calculated using

- 20 (i) the Maxwell Garnett mixing rule (Maxwell Garnett, 1904)
- 25 (ii) the Bruggeman mixing rule (Bruggemann, 1935).

The former treats the vesicles as inclusions in an andesite matrix, while the latter treats vesicles and andesite more symmetrically, assuming that both are inclusions in a matrix with an effective refractive index. More information on effective medium theories can be found in Chylek et al. (2000) and references therein.

20 In Figs. 2 and 3 the extinction (1st row) and scattering efficiencies (2nd row), single-scattering albedo (3rd row), and asymmetry parameter (4th row) for wavelengths of 11 μm (left column) and 12 μm (right column) of ash particles and spheroids with large and small vesicles, respectively, are compared with the spherical models. The results

Infrared signature of realistic volcanic ash particles

A. Kylling et al.

[Title Page](#)

[Abstract](#)

[Introduction](#)

[Conclusions](#)

[References](#)

[Tables](#)

[Figures](#)

[|◀](#)

[▶|](#)

[◀](#)

[▶|](#)

[Back](#)

[Close](#)

[Full Screen / Esc](#)

[Printer-friendly Version](#)

[Interactive Discussion](#)



Infrared signature of realistic volcanic ash particles

A. Kylling et al.

[Title Page](#)[Abstract](#)[Introduction](#)[Conclusions](#)[References](#)[Tables](#)[Figures](#)[|◀](#)[▶|](#)[◀](#)[▶](#)[Back](#)[Close](#)[Full Screen / Esc](#)[Printer-friendly Version](#)[Interactive Discussion](#)

3 Radiative transfer simulations

To calculate the brightness temperature for a nadir viewing satellite the libradtran package was utilized (www.libradtran.org and Mayer and Kylling, 2005). The ash cloud was vertically homogeneous, 1 km thick, and with the cloud top at 10 km. The sub arctic summer atmosphere (Anderson et al., 1986) was adopted as the ambient atmosphere, thus giving a temperature of 225 K at 10 km and a surface temperature of 280 K. The emissivity of the surface was set to 0.98 which is representative for water at the wavelengths considered. Gaseous absorption was treated by the LOWTRAN parameterization (Pierluissi and Peng, 1985; Ricchiazzi et al., 1998). Accurate treatment of the ash particle phase functions were assured by using the improved discrete-ordinate (DISORT) method by Buras et al. (2011) which is based on the versatile and much used DISORT algorithm by Stamnes et al. (1988). Brightness temperatures were calculated for the 11.0 and 12.0 μm (BT11 and BT12, respectively) channels of SEVIRI for various ash optical depths and particle sizes.

15 4 Results

Radiative transfer calculations of the brightness temperature at 11 and 12 μm were made for the various ash particle shapes. Monodispersed particle distributions were used. In Fig. 5 BT11 is shown vs. the brightness temperature difference $\text{dT} = \text{BT11} - \text{BT12}$ for a few representative particle shapes. The solid lines in Fig. 5 represent various particle sizes whose values are indicated in black. The dashed blue lines indicate various ash optical depths whose values are given in blue.

20 The upper left plot is similar to those used to visualize the retrieval of ash mass loading and effective radius from BT11 and BT12 measurements under the assumption of spherical ash particles (Wen and Rose, 1994; Prata and Prata, 2012). The middle and lower left plots show results for the volume-equivalent spheres using the Bruggeman mixing rule for large and small vesicles, respectively. The results for the Bruggeman

AMTD

6, 8937–8958, 2013

Infrared signature of realistic volcanic ash particles

A. Kylling et al.

Title Page	
Abstract	Introduction
Conclusions	References
Tables	Figures
◀	▶
◀	▶
Back	Close
Full Screen / Esc	
Printer-friendly Version	
Interactive Discussion	



mixing rule volume-equivalent spheres are markedly different from those of the mass-equivalent spheres. For the mass-equivalent spheres dBT is negative for sizes smaller than $5\text{ }\mu\text{m}$ in agreement with Wen and Rose (1994). For the volume-equivalent large and small vesicle particles with an effective refractive index based on Bruggeman effective medium theory, dBT is negative for all particles and for particles smaller than about $8\text{ }\mu\text{m}$, respectively. This is also evident in Fig. 6, which shows dBT as a function of particle size for the various particle shapes and ash mass loadings. The sphere models constructed with the Maxwell–Garnett mixing rule gives a similar negative dBT , as indicated in Fig. 6.

The right column in Fig. 5 shows dBT vs. $BT11$ for large vesicle (upper plot), small vesicle (middle plot) and small prolate spheroid (lower plot) ash particles. The results for the other shapes are similar. The ash particles with large (upper right plot) and small (middle right plot) vesicles are qualitatively similar to the volume-equivalent large vesicles particles (middle left plot). The prolate spheroids are qualitatively similar to the volume-equivalent small vesicles particles (lower left plot). However, as shown in Fig. 6, dBT for the ash particles are markedly different compared to both the mass- and volume-equivalent sphere models.

Simulations were also made for a log-normal size distribution with $\sigma = 1.25$. The results exhibit the same general behaviour as shown in Fig. 5 for monodispersed particles.

5 Discussion

Information about volcanic ash in the atmosphere from infrared measurements is deduced in a two-step process. First ash affected pixels are detected, secondly the ash physical properties are retrieved from ash affected pixels.

The detection of ash by the reverse absorption technique is based on the different spectral behaviour of the extinction coefficients of volcanic ash, liquid water and ice cloud and the trace gases in the atmosphere (Prata, 1989). A negative dBT indi-

AMTD

6, 8937–8958, 2013

Infrared signature of realistic volcanic ash particles

A. Kylling et al.

[Title Page](#)

[Abstract](#)

[Introduction](#)

[Conclusions](#)

[References](#)

[Tables](#)

[Figures](#)

◀

▶

◀

▶

[Back](#)

[Close](#)

[Full Screen / Esc](#)

[Printer-friendly Version](#)

[Interactive Discussion](#)



Infrared signature of
realistic volcanic ash
particles

A. Kylling et al.

Title Page	
Abstract	Introduction
Conclusions	References
Tables	Figures
◀	▶
◀	▶
Back	Close
Full Screen / Esc	
Printer-friendly Version	
Interactive Discussion	

cates volcanic ash whereas liquid water and ice clouds give positive dB_T. The non-spherical ash particles in this study give negative brightness temperature difference dB_T for a larger particle size range than for mass-equivalent spherical particles, Figs. 4 and 5. Thus, assuming that the non-spherical particles are a better representation of the real world compared to mass-equivalent spherical particles, nature produces negative dB_T for a larger size range than modelled spherical particles.

The mass loading of a pixel may be calculated as (assuming monodispersed particles, Prata and Prata, 2012)

$$m_l = \frac{4}{3} \rho \frac{r \tau(\lambda)}{Q_{\text{ext}}(\lambda, r)}, \quad (2)$$

where the ash density $\rho = 2600 \text{ kg m}^{-3}$. For a given combination of dB_T and BT₁₁ the optical depth and radius may be found from charts similar to those shown in Fig. 5. Normally spheres, upper left plot, are used for retrieval of ash optical properties. The use of any of the other ash type particles in Fig. 5 will give a different ash mass loading. For example, assuming a measured BT₁₁ = 259.3 K and dB_T = -5.1 K the mass loading is 3.1 and 5.1 g m⁻² for the mass-equivalent sphere model and the ash large vesicle model, respectively. For a thicker ash cloud with BT₁₁ = 233.3 K and dB_T = -20.2 K the corresponding numbers are 7.6 and 9.2 g m⁻². For these two examples the mass-equivalent spherical model retrieves 60 % and 82 % of the mass loading compared to the large vesicles model.

The effect of particle shape may be quantified comparing non-spherical particles and volume-equivalent spherical particles. It is found that for the values of BT₁₁ and BT₁₂ above the volume-equivalent spherical particle model estimated mass loading differs from the ash large vesicle model by about $\pm 25\%$. The difference between the mass loading retrieved with mass-equivalent spherical particles and porous ash particles may be compared with the uncertainty arising from lack of knowledge of other factors (surface temperature, surface emissivity, plume geometry and altitude, aerosol type, atmospheric water vapor) affecting the ash mass loading. Corradini et al. (2008) have

estimated that typical errors in total mass estimates due to these other factors are on the order of 40 %. The error made by assuming spherical ash particles will depend on the amount of ash, its size distribution and altitude. However, from the above mass loading estimates it may be argued that inclusion of the uncertainty in ash particle shape in the total mass error estimate, will increase the total mass error estimate to 5 45–50 %.

6 Conclusions

Optical properties have been calculated for highly irregular and porous ash particles with refractive indices relevant for the thermal infrared. Brightness temperatures at 11

10 and 12 μm as measured by an Earth-viewing satellite have been calculated for irregular and porous ash particles, and volume-equivalent and mass-equivalent spheres. It was found that:

1. Optical properties of non-spherical ash particles differ significantly from mass-equivalent spherical particles in the IR. Optical properties of volume-equivalent spherical ash particles differ significantly from mass-equivalent spherical particles in the IR.
- 15 2. Mass-equivalent spherical particles produce a negative dB_T for a narrower particle size range (up to 5 μm) than volume-equivalent spherical particles and non-spherical particles (up to 10 μm). This indicates that in reality a wider range of ash particles are detectable by the inverse absorption technique method than indicated by spherical model calculations.
- 20 3. For ash mass loading retrieval mass-equivalent spherical particles will give less mass (up to 40 % for examples presented here) compared to non-spherical particles.

[Title Page](#)

[Abstract](#)

[Introduction](#)

[Conclusions](#)

[References](#)

[Tables](#)

[Figures](#)

[|◀](#)

[▶|](#)

[◀](#)

[▶](#)

[Back](#)

[Close](#)

[Full Screen / Esc](#)

[Printer-friendly Version](#)

[Interactive Discussion](#)



4. The difference between volume-equivalent spherical particles and non-spherical particles brightness temperature gives differences in retrieved ash mass loading of about $\pm 25\%$.

5. The uncertainty in the particle shape increases the error in the total mass from about 40 % to about 45–50 %.

It is noted that ash particle shape is not usually known for an on-going volcanic eruption. Thus, for operational monitoring of ongoing volcanic eruptions it is preferable to assume spherical ash particles and rather increase the uncertainty in the mass estimate. To further quantify the uncertainty due to the assumption of particle shape it

10 would be useful in future work to compare non-spherical and spherical retrievals for real volcanic episodes.

Acknowledgements. B. Draine and M. Mishchenko are acknowledged for making their respective light scattering programs publicly available. M. Kahnert acknowledges funding from the Swedish Research Council (Vetenskapsrådet) under project 621-2011-3346. H. Lindqvist and T. Nousiainen acknowledge funding from the Academy of Finland under project 125180. A. Kylling acknowledges support from the FP7 project FUTUREVOLC “A European volcanological supersite in Iceland: a monitoring system and network for the future”, (Grant agreement no: 308377) and the Norwegian Research Council (Contract 224716/E10).

References

20 Anderson, G., Clough, S., Kneizys, F., Chetwynd, J., and Shettle, E.: AFGL Atmospheric Constituent Profiles (0–120 km), Tech. Rep. AFGL-TR-86-0110, Air Force Geophys. Lab., Hanscom Air Force Base, Bedford, Mass., 1986. 8945

Bruggemann, D. A. G.: Berechnung verschiedener physikalischer Konstanten von heterogenen Substanzen. 1. Dielektrizitätskonstanten und Leitfähigkeiten der Mischkörper aus isotropen Substanzen, Ann. Phys., 24, 636–664, 1935. 8943

25 Buras, R., Dowling, T., and Emde, C.: New secondary-scattering correction in DISORT with increased efficiency for forward scattering, J. Quant. Spectrosc. Ra., 112, 2028–2034, doi:10.1016/j.jqsrt.2011.03.019, 2011. 8945

[Title Page](#)

[Abstract](#)

[Introduction](#)

[Conclusions](#)

[References](#)

[Tables](#)

[Figures](#)

◀

▶

[Back](#)

[Close](#)

[Full Screen / Esc](#)

[Printer-friendly Version](#)

[Interactive Discussion](#)



Chylek, P., Videen, G., Geldart, D. J. W., Dobbie, J. S., and Tso, H. C. W.: Effective medium approximations for heterogeneous particles, in: *Light Scattering by Nonspherical Particles*, edited by: Mishchenko, M. I., Hovenier, J. W., and Travis, L. D., Academic Press, San Diego, 274–308, 2000. 8943

5 Clarisse, L., Hurtmans, D., Prata, A. J., Karagulian, F., Clerbaux, C., Maziére, M. D., and Coheur, P.-F.: Retrieving radius, concentration, optical depth, and mass of different types of aerosols from high-resolution infrared nadir spectra, *Appl. Optics*, 49, 3713–3722, 2010. 8938

10 Corradini, S., Spinette, C., Carboni, E., Tirelli, C., Buongiorno, M. F., Pugnaghi, S., and Gangale, G.: Mt. Etna tropospheric ash retrieval and sensitivity analysis using Moderate Resolution Imaging Spectroradiometer Measurements, *J. Appl. Remote Sens.*, 2, 023550, doi:10.11117/1.3046674, 2008. 8947

15 Drain, B. T. and Flatau, P. J.: Discrete dipole approximation for scattering calculations, *J. Opt. Soc. Am.*, 11, 1491–1499, 1994. 8942

20 Drain, B. T. and Flatau, P. J.: User Guide to the Discrete Dipole Approximation Code DDSCAT 7.2, available at: <http://arXiv.org/abs/1202.3424> (last access: 14 October 2013), 2012. 8942

Kahnert, M., Nousiainen, T., and Mauno, P.: On the impact of non-sphericity and small-scale surface roughness on the optical properties of hematite aerosols, *J. Quant. Spectrosc. Ra.*, 112, 1815–1824, 2011. 8939

25 Kahnert, M., Nousiainen, T., Thomas, M. A., and Tyynelä, J.: Light scattering by particles with small-scale surface roughness: comparison of four classes of model geometries, *J. Quant. Spectrosc. Ra.*, 113, 2356–2367, 2012. 8939

Krotkov, N., Flittner, D., Krueger, A., Kostinski, A., Riley, C., Rose, W., and Torres, O.: Effect of particle non-sphericity on satellite monitoring of drifting volcanic ash clouds, *J. Quant. Spectrosc. Ra.*, 63, 613–630, doi:10.1016/S0022-4073(99)00041-2, 1999. 8939

30 Lindqvist, H., Muinonen, K., and Nousiainen, T.: Light scattering by coated Gaussian and aggregate particles, *J. Quant. Spectrosc. Ra.*, 110, 1398–1410, 2009. 8941

Lindqvist, H., Nousiainen, T., Zubko, E., and Muñoz, O.: Optical modeling of vesicular volcanic ash particles, *J. Quant. Spectrosc. Ra.*, 112, 1871–1880, doi:10.1016/j.jqsrt.2011.01.032, 2011. 8940, 8942

Maxwell Garnett, J. C.: Colours in metal glasses and in metallic films, *Philos. T. R. Soc. A*, 203, 385–420, 1904. 8943

Infrared signature of realistic volcanic ash particles

A. Kylling et al.

[Title Page](#)

[Abstract](#)

[Introduction](#)

[Conclusions](#)

[References](#)

[Tables](#)

[Figures](#)

◀

▶

◀

▶

[Back](#)

[Close](#)

[Full Screen / Esc](#)

[Printer-friendly Version](#)

[Interactive Discussion](#)



Mayer, B. and Kylling, A.: Technical note: The libRadtran software package for radiative transfer calculations – description and examples of use, *Atmos. Chem. Phys.*, 5, 1855–1877, doi:10.5194/acp-5-1855-2005, 2005. 8945

5 Mishchenko, M. I.: Electromagnetic scattering by nonspherical particles: a tutorial review, *J. Quant. Spectrosc. Ra.*, 110, 808–832, 2009. 8938

Mishchenko, M. I., Travis, L. D., and Lacis, A. A.: *Scattering, Absorption, and Emission of Light by Small Particles*, Cambridge University Press, Cambridge, 2002. 8942

Muinonen, K., Zubko, E., Tyynelä, J., Shkuratov, Y. G., and Videen, G.: Light scattering by Gaussian random particles with discrete-dipole approximation, *J. Quant. Spectrosc. Ra.*, 106, 360–377, 2007. 8941

Newman, S. M., Clarris, L., Hurtmans, D., Marenco, F., Johnson, B., Turnbull, K., Havemann, S., Baran, A. J., O'Sullivan, D., and Haywood, J.: A case study of observations of volcanic ash from the Eyjafjallajökull eruption: 2. Airborne and satellite radiative measurements, *J. Geophys. Res.*, 117, D00U13, doi:10.1029/2011JD016780, 2012. 8939

15 Nousiainen, T., Kahnert, M., and Lindqvist, H.: Can particle shape information be retrieved from light-scattering observations using spheroidal model particles?, *J. Quant. Spectrosc. Ra.*, 112, 2213–2225, doi:10.1016/j.jqsrt.2011.05.008, 2011. 8940, 8942

Pavolos, M. J., Heidinger, A. K., and Sieglaff, J.: Automated retrievals of volcanic ash and dust cloud properties from upwelling infrared measurements, *J. Geophys. Res.*, 118, 1–23, doi:10.1002/jgrd.50173, 2013. 8938

Pierluissi, J. H. and Peng, G.-S.: New molecular transmission band models for LOWTRAN, *Opt. Eng.*, 24, 541–547, 1985. 8945

Pollack, J. B., Toon, O. B., and Khare, B. N.: Optical properties of some terrestrial rocks and glasses, *ICARUS*, 19, 372–389, 1973. 8939

25 Prata, A. J.: Infrared radiative transfer calculations for volcanic ash clouds, *Geophys. Res. Lett.*, 16, 1293–1296, 1989. 8938, 8946

Prata, A. J. and Prata, A. T.: Eyjafjallajökull volcanic ash concentrations determined using Spin Enhanced Visible and Infrared Imager measurements, *J. Geophys. Res.*, 117, D00U23, doi:10.1029/2011JD016800, 2012. 8938, 8945, 8947

30 Ricchiazzi, P., Yang, S., Gautier, C., and Sowle, D.: SBDART: a research and Teaching software tool for plane-parallel radiative transfer in the Earth's atmosphere, *B. Am. Meteorol. Soc.*, 79, 2101–2114, 1998. 8945

Infrared signature of
realistic volcanic ash
particles

A. Kylling et al.

[Title Page](#)

[Abstract](#)

[Introduction](#)

[Conclusions](#)

[References](#)

[Tables](#)

[Figures](#)

◀

▶

◀

▶

[Back](#)

[Close](#)

[Full Screen / Esc](#)

[Printer-friendly Version](#)

[Interactive Discussion](#)



Stamnes, K., Tsay, S.-C., Wiscombe, W., and Jayaweera, K.: Numerically stable algorithm for discrete-ordinate-method radiative transfer in multiple scattering and emitting layered media, *Appl. Optics*, 27, 2502–2509, 1988. 8945

5 Wen, S. and Rose, W. I.: Retrieval of sizes and total masses of particles in volcanic clouds using AVHRR bands 4 and 5, *J. Geophys. Res.*, 99, 5421–5431, 1994. 8938, 8945, 8946

Yang, P., Feng, Q., Hong, G., Kattawar, G. W., Wiscombe, W. J., Mishchenko, M. I., Dubovik, O., Laszlo, I., and Sokolik, I. N.: Modeling of the scattering and radiative properties of nonspherical dust-like aerosols, *J. Aerosol Sci.*, 38, 995–1014, 2007. 8939

Infrared signature of realistic volcanic ash particles

A. Kylling et al.

[Title Page](#)

[Abstract](#)

[Introduction](#)

[Conclusions](#)

[References](#)

[Tables](#)

[Figures](#)

[|◀](#)

[▶|](#)

[◀](#)

[▶](#)

[Back](#)

[Close](#)

[Full Screen / Esc](#)

[Printer-friendly Version](#)

[Interactive Discussion](#)



Infrared signature of
realistic volcanic ash
particles

A. Kylling et al.

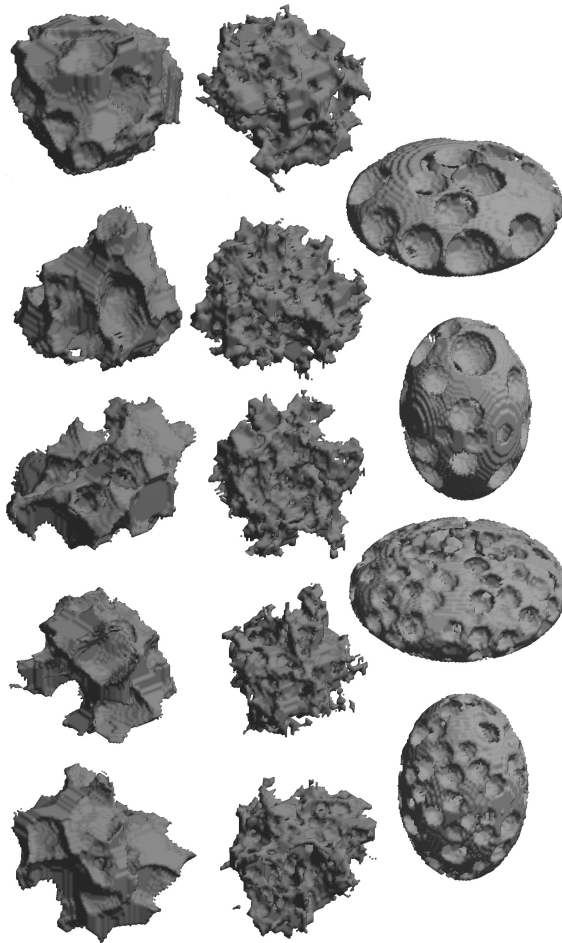


Fig. 1. (left column) Ash particles with large vesicles. (middle column) Ash particles with small vesicles. (right column) Prolate and oblate spheroids with large and small vesicles.

Title Page	Abstract	Introduction
Conclusions	References	
Tables	Figures	
◀	▶	
◀	▶	
Back	Close	
Full Screen / Esc		
Printer-friendly Version		
Interactive Discussion		

Infrared signature of
realistic volcanic ash
particles

A. Kylling et al.

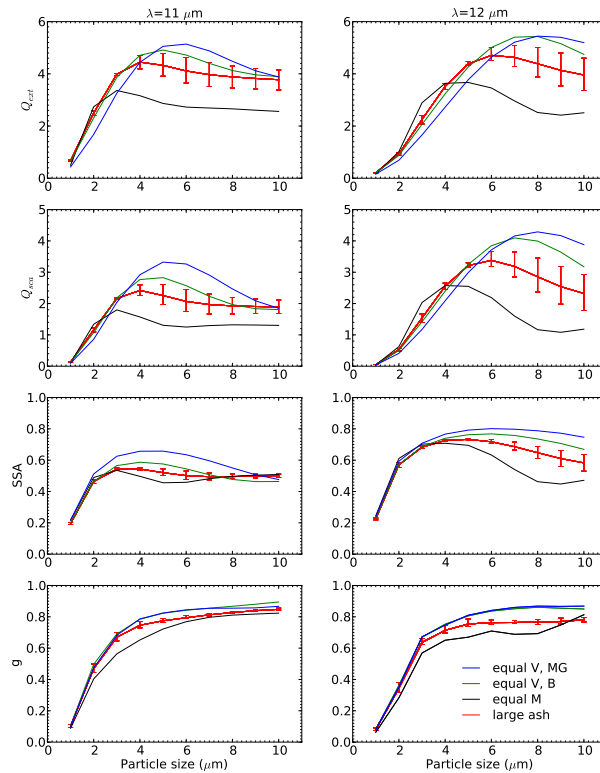


Fig. 2. Optical properties of large vesicle ash particles and sphere models. The extinction (1st row), scattering efficiencies (2nd row), single-scattering albedo (3rd row), and asymmetry parameter (4th row) are shown for wavelengths of $11\text{ }\mu\text{m}$ (left column) and $12\text{ }\mu\text{m}$ (right column). The mass-equivalent (equal M) spheres are shown in black, the volume-equivalent spheres using the Bruggeman mixing rule (equal V , B) in green and the volume-equivalent spheres using the Maxwell Garnett mixing rule (equal V , MG) in blue. The red lines represents the average of the non-spherical ash particles with the error bars representing the minimum and maximum values.

Infrared signature of
realistic volcanic ash
particles

A. Kylling et al.

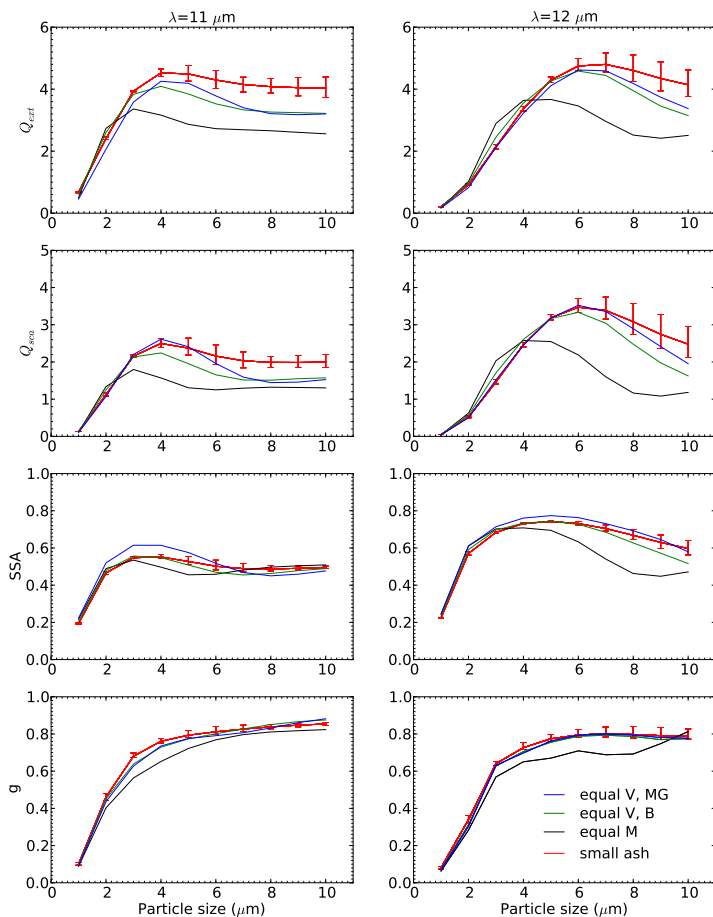


Fig. 3. Similar to Fig. 2 but for small vesicle ash particles.

[Title Page](#)[Abstract](#)[Introduction](#)[Conclusions](#)[References](#)[Tables](#)[Figures](#)[|◀](#)[▶|](#)[◀](#)[▶](#)[Back](#)[Close](#)[Full Screen / Esc](#)[Printer-friendly Version](#)[Interactive Discussion](#)

Infrared signature of
realistic volcanic ash
particles

A. Kylling et al.

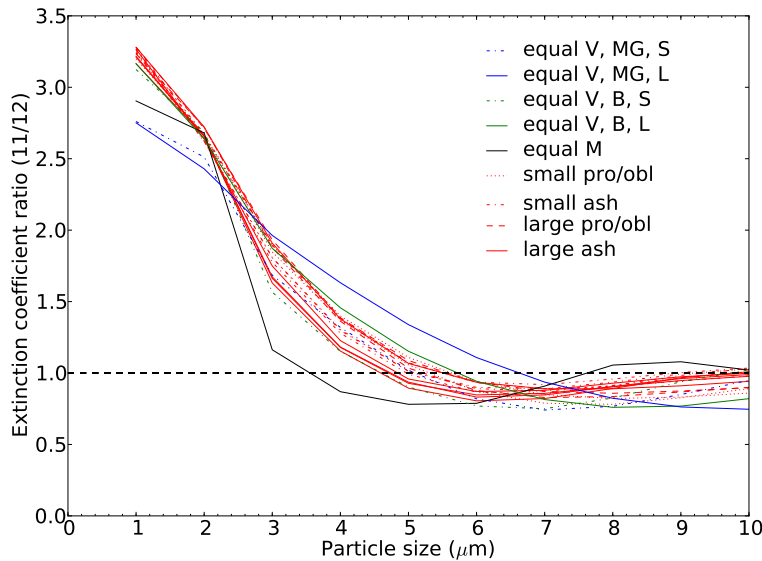


Fig. 4. The ratio of the extinction coefficients at 11.0 and 12.0 μm for the various particle shapes.

Infrared signature of
realistic volcanic ash
particles

A. Kylling et al.

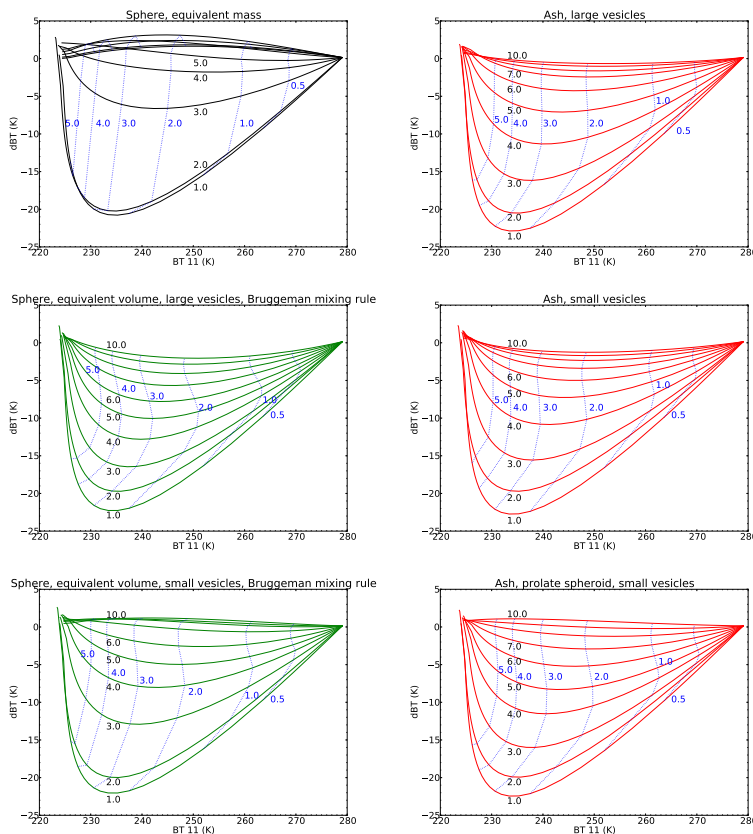


Fig. 5. The brightness temperature at 11 μm vs. the brightness temperature difference for various model ash particle types. Black colored numbers label particle size (μm) isolines (black). Blue numbers are ash cloud optical depth (dashed blue lines).

- [Title Page](#)
- [Abstract](#) [Introduction](#)
- [Conclusions](#) [References](#)
- [Tables](#) [Figures](#)
- [◀](#) [▶](#)
- [◀](#) [▶](#)
- [Back](#) [Close](#)
- [Full Screen / Esc](#)
- [Printer-friendly Version](#)
- [Interactive Discussion](#)

Infrared signature of
realistic volcanic ash
particles

A. Kylling et al.

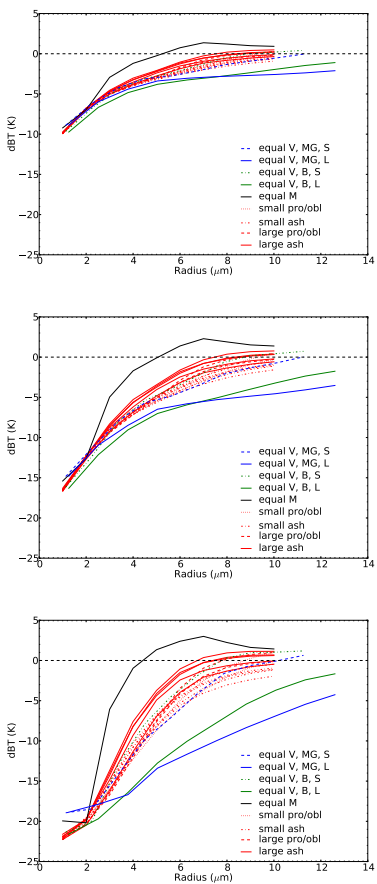


Fig. 6. The brightness temperature difference as a function of particle size for ash cloud optical depths of 0.5 (top), 1.0 (middle) and 3.0 (bottom).